Journal of Solid Mechanics Vol. 12, No. 2 (2020) pp. 315-333
DOI: 10.22034/jsm.2019.1865985.1420

# Free Vibration and Transient Response of Heterogeneous Piezoelectric Sandwich Annular Plate Using Third-Order Shear Deformation Assumption

P. Roodgar Saffari [1], M. Fakhraie [1,*] , M.A. Roudbari [2,3]

[1]*Department of Mechanical Engineering, Lahijan Branch, Islamic Azad University, Lahijan, Iran*
[2]*Department of Mechanical Engineering, University of Guilan, Rasht, Iran*
[3]*Department of Civil Engineering, Zhejiang University, Hangzhou 310058, People's Republic of China, China*

Received 11 February 2020; accepted 3 April 2020

**ABSTRACT**
Based on the third-order shear deformation theory (TSDT), this paper numerically investigates the natural frequencies and time response of three-layered annular plate with functionally graded materials (FGMs) sheet core and piezoelectric face sheets, under initial external electric voltage. The impressive material specifications of FGM core are assumed to vary continuously across the plate thickness utilizing a power law distribution. The equilibrium equations are obtained employing Hamilton's method and then solved applying differential quadrature method (DQM) in conjunction with Newmark-β. Numerical studies are carried out to express the influences of the external electric voltage, aspect ratio, and material gradient on the variations of the natural frequencies and time response curves of FGM piezoelectric sandwich annular plate. It is precisely shown that these parameters have considerable effects on the free vibration and transient response.


**Keywords:** Transient response; Three-layered plate; Piezoelectric; FGMs; TSDT.

## 1 INTRODUCTION

SMART materials such as piezoelectric and magneto-electro-elastic can significantly change their mechanical and physical properties under various external excitations such as electric or magnetic fields. Piezoelectric materials are a significant category of the intelligent materials which, by exposing them under mechanical deformations, the electrical charge can be produced (direct effect). In addition, when an electric field is applied to the piezoelectric materials, the mechanical stresses can be produced (reverse effect). Liu et al. [1] analyzed free vibration of thick circular plate integrated with piezoelectric layers via first shear deformation theory (FSDT) under different boundary conditions. Based upon the higher-order shear deformation theory conjunction with finite

*Corresponding author. Tel.: +98 9111321248.
*E-mail address: fakhraie@liau.ac.ir* (M. Fakhraie).

element method, Dash and Singh [2] studied nonlinear natural frequencies of geometrically nonlinear shear deformable piezoelectric laminated plate. Phung-Van et al. [3] presented a simple and effective technique based upon the combination of isogeometric analysis and TSDT to study static, free vibration and dynamic behaviors composite plates integrated with piezoelectric sensors and actuators. Kuang et al. [4] implemented the theoretical processor to obtain piezoelectric material parameters and the characteristic functions of the natural frequency of piezoelectric circular plate. Based on the flexural wave equation of thin circular plate and the transfer matrix method, Shu et al. [5] investigated theoretically and numerically the behavior of flexural waves propagating. Khorshidvand et al. [6] derived buckling loads for solid circular plates subjected to the uniform radial compressive loading under the clamped edge condition. In addition, several works on the static, dynamic behaviors of piezoelectric plates have been performed, see for example [7-13]. During 1984-1985, in Japan, to omit the singular stresses and improve the thermal and mechanical stability, a group of material researches proposed a specific class of advanced heterogeneous materials called FGMs. FGMs encompass the heterogeneous feature and persistent variation of material characteristics from one surface to the other [14]. Until today, many investigation projects have been conducted to investigate the application of FGMs in engineering smart structures. Bhangale and Ganesan [15] used power law model to study the effect of FGMs on the changes of the natural frequencies of magneto-electro-elastic finite cylindrical shells. The authors supposed that the material characteristics of the cylindrical shell vary in the thickness. According to the power law distribution and FSDT, the effect of environment temperature and material gradient on the sound radiation of FGM plate subjected to point load is demonstrated by Yang et al. [16]. Su et al. [17] performed free vibration and transient response of FG piezoelectric plate with various boundary conditions using FSDT. They showed that an increase in the value of gradient index leads to the increase of response magnitude. Kiani [18] analyzed free vibration characteristics of carbon nanotube reinforced composite (CNTRC) plates integrated with piezoelectric layers at the bottom and top surfaces. Barati and Zenkour [19] employed a refined four-variable plate theory for modeling of the electro-thermo-mechanical vibrational properties of FG piezoelectric plates with porosities and different boundary conditions. Smart composite sandwich plates are finding an increasing role in car manufacturing, vibration suppression, vibro-acoustic, because of their good specific stiffness and damping properties. The use of these structures allows decreasing structures' weight without compromising stiffness, this helps developing engineering structures with improved performances. Despite the thickness of the core layer, sandwich plates are light and have a relatively high flexural strength. In addition, by using piezoelectric layers as sensor and actuator, the vibration behavior of many engineering structures can be controlled. Because of the superior mechanical characteristics and excellent vibration insulation performance of sandwich structures over single-wall structures in aviation, marine and civil industries, numerous researchers experimentally and analytically have focused on the sandwich structures behaviors [20-23]. For example, based on the hyperbolic shear deformation theory, El Meiche et al. [24] investigated the buckling and free vibration of FG sandwich rectangular plate. Hadji et al. [25] analyzed vibration response of FGM sandwich plate via the four-variable refined plate approach. The authors reported that four-variable refined plate theory is accurate and simple in solving the free vibration behavior. Dinh Duc and Hong Cong [26] studied the nonlinear dynamic response of imperfect FG sandwich plates with integrated piezoelectric layers resting on elastic substrate in thermal environment employing higher-order shear deformation plate theory. According to Lord–Shulman theory and utilizing Fourier series state space technique, Alibeigloo [27] carried out the three dimensional transient coupled thermo-elastic problem of simply supported sandwich rectangular plate under thermal shock. Fatahi-Vajari and Imam [28] studied the lateral vibration of single-layered graphene sheets based on a new theory called doublet mechanics. Fazzolari [29] examined buckling behavior of FGM sandwich plate by virtue of the hierarchical trigonometric Ritz formulation. Arefi et al. [30] applied two-variable sinusoidal shear deformation theory in conjunction with nonlocal piezo elasticity relations for free vibration analysis of a sandwich Nanoplate.

The past review of the literatures evidently demonstrates that free vibration and transient response of piezoelectric FG annular sandwich plate using TSDT excited with a uniform mechanical load on the top surface has not been studied. The main purpose of present work is to fill this gap in the literature. The impressive material characteristics of FG core annular plate are supposed to be continuously variable across the plate thickness using a power law model. Hamilton's method is applied to earn the equilibrium equations of the system and then are solved with differential quadrature method (DQM) in conjunction with Newmark-$\beta$. Finally, numerical studies are carried out to show the effects of some factors such as electric voltage, FG core plate thickness, inner radius, and material gradient on the time response of FG piezoelectric sandwich annular plate.

## 2 THEORY AND FORMULATION

### *2.1 Problem configuration*

Fig. 1 schematically illustrates the proposed problem configuration along with the cylindrical coordinate system ($r,\theta$, $z$). Suppose an annular sandwich plate (inner radius $R_1$ ; outer radius $R_2$ ) composed of FGM core (uniform thickness $h_e$ ) and the two piezoelectric face-sheets (uniform thickness $h_p$ ).

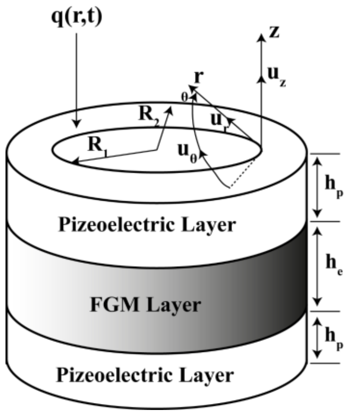


**Fig.1**
The Schematic and coordinate system of a FGM piezoelectric sandwich plate.

### *2.2 Basic formulations*

#### *2.2.1 FGM relations*

In the present study, the impressive material characteristics of FGM core annular plate are presented based according to the power law model as follows [31]

$$
\begin{aligned}
E(z) &= E_c + (E_m - E_c)\left(\frac{1}{2}+\frac{z}{h_e}\right)^k \\
\rho(z) &= \rho_c + (\rho_m - \rho_c)\left(\frac{1}{2}+\frac{z}{h_e}\right)^k
\end{aligned}
\tag{1}
$$

where subscripts *m* and *c* are, respectively, metal and ceramic terms. The material gradient index is expressed with $k \geq 0$. Furthermore, *E* and $\rho$ indicate, respectively, Young's modulus and mass density.

#### *2.2.2 Deflection field*

Based upon TSDT of Reddy [32], the deflection field $(u_r, u_\theta, u_z)$ based on the cylindrical coordinate at an arbitrary spot for FGM core annular plate along the axes ($r,\theta$, $z$) can be presented as:

$$
\begin{aligned}
& u_r(r,z,t) = u_0(r,t) + z\,\theta_r(r,t) - \frac{4z^3}{3h^2}\left(\theta_r(r,t) + \frac{\partial w_0(r,t)}{\partial r}\right), \; h = \frac{h_e}{2} + h_p \\
& u_c(r,z,t) = 0 \\
& u_z(r,z,t) = w_0(r,t)
\end{aligned}
\tag{2}
$$

where $u_0$ and $w_0$ show mid-plane displacements of sandwich plate and $\theta_r$ refers to the rotation displacements of middle surface of sandwich plate about *r-z* plane.

*2.2.3 Strains*

Utilizing Eq. (2), the linear strain components are denoted as [33]

$$
\begin{aligned}
\varepsilon_{rr} &= \frac{\partial u_r}{\partial r} = \frac{\partial u_0}{\partial r} - \frac{4z^3}{3h^2}\left(\frac{\partial \theta_r}{\partial r} + \frac{\partial^2 w_0(r,t)}{\partial r^2}\right) \\
\varepsilon_{\theta\theta} &= \frac{u_r}{r} + \frac{1}{r}\frac{\partial u_\theta}{\partial \theta} = \frac{u_0}{r} + \frac{z\,\theta_r}{r} - \frac{4z^3}{3rh^2}\left(\theta_r + \frac{\partial w_0}{\partial r}\right) \\
\gamma_{rz} &= \frac{\partial u_r}{\partial z} + \frac{\partial u_z}{\partial r} = \left(1 - \frac{4z}{h^2}\right)\left(\theta_r + \frac{\partial w_0}{\partial r}\right)
\end{aligned}
\tag{3}
$$

In which $\varepsilon_{rr}$ and $\varepsilon_{\theta\theta}$ denote the normal strains components, and $\gamma_{rz}$ is shear strain term. By taking into account the plane stress assumption and assuming the linear behavior of FGM, the constitutive stress-strain relations for inhomogeneous core plate can be expressed as below [34]

$$
\begin{bmatrix} \sigma_{rr}^e \\ \sigma_{\theta\theta}^e \\ \sigma_{rz}^e \end{bmatrix} = \begin{bmatrix} \frac{E(z)}{1-\nu^2} & \frac{\nu E(z)}{1-\nu^2} & 0 \\ \frac{\nu E(z)}{1-\nu^2} & \frac{E(z)}{1-\nu^2} & 0 \\ 0 & 0 & \frac{E(z)}{2(1+\nu)} \end{bmatrix} \begin{bmatrix} \varepsilon_{rr} \\ \varepsilon_{\theta\theta} \\ \gamma_{rz} \end{bmatrix}
\tag{4}
$$

where $\sigma_{rr}$ and $\sigma_{\theta\theta}$ demonstrate the normal stress components. Also, $\sigma_{rz}$ refers to the shear stress, and $\nu$ is Poisson's ratio. Furthermore, the constitutive stress-strain relations for piezoelectric face sheets can be written as:

$$
\begin{aligned}
\begin{bmatrix} \sigma_{rr}^p \\ \sigma_{\theta\theta}^p \\ \sigma_{rz}^p \end{bmatrix} &= \begin{bmatrix} \bar{c}_{11} & \bar{c}_{11} & 0 \\ \bar{c}_{21} & \bar{c}_{22} & 0 \\ 0 & 0 & \bar{c}_{44} \end{bmatrix} \begin{bmatrix} \varepsilon_{rr} \\ \varepsilon_{\theta\theta} \\ \gamma_{rz} \end{bmatrix} - \begin{bmatrix} 0 & 0 & \bar{e}_{31} \\ 0 & 0 & \bar{e}_{32} \\ \bar{e}_{15} & 0 & 0 \end{bmatrix} \begin{bmatrix} E_r \\ E_\theta \\ E_z \end{bmatrix} \\
\begin{bmatrix} D_r^p \\ D_\theta^p \\ D_z^p \end{bmatrix} &= \begin{bmatrix} 0 & 0 & \bar{e}_{15} \\ 0 & 0 & 0 \\ \bar{e}_{31} & \bar{e}_{32} & 0 \end{bmatrix} \begin{bmatrix} \varepsilon_{rr} \\ \varepsilon_{\theta\theta} \\ \gamma_{rz} \end{bmatrix} + \begin{bmatrix} \bar{k}_{11} & 0 & 0 \\ 0 & 0 & 0 \\ 0 & 0 & \bar{k}_{33} \end{bmatrix} \begin{bmatrix} E_r \\ E_\theta \\ E_z \end{bmatrix}
\end{aligned}
\tag{5}
$$

where $\begin{bmatrix} D_r & D_\theta & D_z \end{bmatrix}^T$ is the electric displacement tensor for piezoelectric layers, $\begin{bmatrix} E_r & E_\theta & E_z \end{bmatrix}^T$ demonstrates the electric field tensor. Also, $\bar{c}_{ij}$ , $\bar{e}_{ij}$ and $\bar{k}_{ij}$ are the reduced material constants, and defining, respectively, as elastic, piezoelectric constants, and dielectric which can be denoted as follows:

$$
\begin{aligned}
&\bar{c}_{11} = c_{11} - \frac{c_{13}^2}{c_{33}} ,\ \bar{c}_{12} = c_{12} - \frac{c_{13}c_{23}}{c_{33}} ,\ \bar{c}_{22} = c_{22} - \frac{c_{23}^2}{c_{33}} \\
&\bar{c}_{44} = c_{44} ,\ \bar{c}_{55} = c_{55} ,\ \bar{e}_{31} = e_{31} - \frac{c_{13}e_{33}}{c_{33}} \\
&\bar{e}_{15} = e_{15} ,\ \bar{e}_{32} = e_{32} - \frac{c_{23}e_{33}}{c_{33}} ,\ \bar{k}_{11} = k_{11} ,\ \bar{k}_{33} = k_{33} + \frac{e_{33}^2}{c_{33}}
\end{aligned}
\tag{6}
$$

The relevant boundary conditions of the electric fields at top and bottom planes of each piezoelectric face sheet are as:

$$
\phi\left(r, \pm\left\{\frac{h_e}{2} + h_p\right\}, t\right) = V \qquad \phi\left(r, \pm\left\{\frac{h_e}{2}\right\}, t\right) = -V
\tag{7}
$$

where $V$ refers to the external electric voltage. As well as, with respect to the electric boundary condition (Eq. (7)), the distribution of electric potential through the thickness of each piezoelectric face sheet is supposed as a function of cosine and linear variation as [35]

$$\phi(r,z,t)=-\cos(\pi\frac{z-\frac{h_e}{2}-\frac{h_p}{2}}{h_p})\varphi(r,t)+2\frac{(z-\frac{h_e}{2}-\frac{h_p}{2})}{h_p}V \tag{8}$$

where $\varphi(r,t)$ is the electric potential variations of the mid-plane along $r$ direction for each piezoelectric annular layer. Furthermore, to satisfy Maxwell relationships, the electric field should be function of the negative gradient of electric potential $\phi(r,z,t)$ as follows:

$$\begin{aligned}E_r&=-\frac{\partial\phi(r,z,t)}{\partial r}=\cos(\pi\frac{z-\frac{h_e}{2}-\frac{h_p}{2}}{h_p})\frac{\partial\varphi(r,t)}{\partial r}\\E_z&=-\frac{\partial\phi(r,z,t)}{\partial z}=-\frac{\pi}{h_p}\sin(\pi\frac{z-\frac{h_e}{2}-\frac{h_p}{2}}{h_p})\varphi-\frac{2V}{h_p}\end{aligned} \tag{9}$$

*2.3 Governing partial equations*

To obtain the equation of motion, Hamilton's principle is used in the form

$$\int_0^t(\delta T-\delta U-\delta W_{ext})dt=0 \tag{10}$$

In which $\delta U$, $\delta W_{ext}$ and $\delta T$ are, respectively, the total virtual strain energy variation, the external work variation and the kinetic energy variation, which applying TSDT (Eq. (2)) can be expressed in Appendix A.

Finally, by inserting expressions (A.3), (A.5) and (A.7) in Hamilton's equation, after integrating by parts, the equations of motion for the FG piezoelectric sandwich plate are obtained as:

$$\begin{aligned}&\delta u_0\Rightarrow\frac{\partial N_{rr}^{ABC}}{\partial r}+\frac{N_{rr}^{ABC}}{r}-\frac{N_{\theta\theta}^{ABC}}{r}=I_0\ddot{u}_0+I_1\ddot{\theta}_r-I_3c_1\ddot{\theta}_r-I_3c_1\frac{\partial\ddot{w}_0}{\partial r},\\&\delta w_0\Rightarrow\frac{c_1\partial^2p_{rr}^{ABC}}{\partial r^2}+2\frac{c_1\partial p_{rr}^{ABC}}{r\partial r}-\frac{c_1\partial p_{\theta\theta}^{ABC}}{r\partial r}+\frac{\partial Q_{rz}^{ABC}}{\partial r}-3c_1\frac{\partial R_{rz}^{ABC}}{\partial r}+\frac{Q_{rz}^{ABC}}{r}-3c_1\frac{R_{rz}^{ABC}}{r}+\left(N^P\right)\left(\frac{\partial^2w_0}{\partial r^2}+\frac{\partial w_0}{r\partial r}\right)\\&=q+I_0\ddot{w}_0+I_3c_1\frac{\partial\ddot{w}_0}{\partial r}+I_3c_1\frac{\ddot{u}_0}{r}+I_4c_1\frac{\partial\ddot{\theta}_r}{\partial r}+I_4c_1\frac{\ddot{\theta}_r}{r}-I_6c_1^2\frac{\partial\ddot{\theta}_r}{\partial r}-I_6c_1^2\frac{\ddot{\theta}_r}{r}-I_6c_1^2\frac{\partial^2\ddot{w}_0}{\partial r^2}-I_6c_1^2\frac{\partial\ddot{w}_0}{r\partial r},\\&\delta\theta_r\Rightarrow\frac{\partial M_{rr}^{ABC}}{\partial r}-c_1\frac{\partial p_{rr}^{ABC}}{\partial r}+\frac{M_{rr}^{ABC}}{r}-c_1\frac{p_{rr}^{ABC}}{r}-\frac{M_{\theta\theta}^{ABC}}{r}+c_1\frac{p_{\theta\theta}^{ABC}}{r}-Q_{rz}^{ABC}+3c_1R_{rz}^{ABC}=\\&I_1\ddot{u}_0+I_2\ddot{\theta}_r-I_3c_1\ddot{u}_0-2I_4c_1\ddot{\theta}_r+I_6c_1^2\ddot{\theta}_r-I_4c_1\frac{\partial\ddot{w}_0}{\partial r}+I_6c_1^2\frac{\partial\ddot{w}_0}{\partial r},\\&\delta\varphi\Rightarrow\int_{-\frac{h_e}{2}-h_p}^{-\frac{h_e}{2}}\left[\frac{\partial D_r}{\partial r}\cos(\pi\frac{z-\frac{h_e}{2}-\frac{h_p}{2}}{h_p})+\frac{D_r}{r}\cos(\pi\frac{z-\frac{h_e}{2}-\frac{h_p}{2}}{h_p})+\frac{\partial D_z}{\partial z}(\frac{\pi}{h_p})\sin(\pi\frac{z-\frac{h_e}{2}-\frac{h_p}{2}}{h_p})\right]dz+\\&\int_{\frac{h_e}{2}}^{\frac{h_e}{2}+h_p}\left[\frac{\partial D_r}{\partial r}\cos(\pi\frac{z-\frac{h_e}{2}-\frac{h_p}{2}}{h_p})+\frac{D_r}{r}\cos(\pi\frac{z-\frac{h_e}{2}-\frac{h_p}{2}}{h_p})+\frac{\partial D_z}{\partial z}(\frac{\pi}{h_p})\sin(\pi\frac{z-\frac{h_e}{2}-\frac{h_p}{2}}{h_p})\right]dz\end{aligned} \tag{11}$$

where $ABC = A + B + C$ . By employing Eq.(A.6) into Eq. (11), the coupled governing equations are rewritten as:

$$
\begin{aligned}
&\delta u_0 \Rightarrow\ A_{11}\left(\frac{\partial^2 u_0}{\partial r^2}+\frac{\partial u_0}{r\partial r}-\left(1-\frac{A_{12}}{A_{11}}\right)\frac{u_0}{r^2}\right)+B_{11}\left(\frac{\partial^2\theta_r}{\partial r^2}+\frac{\partial\theta_r}{r\partial r}-\left(1-\frac{B_{12}}{B_{11}}\right)\frac{\theta_r}{r^2}\right)\\
&-D_{11}c_1\left(\frac{\partial^2\theta_r}{\partial r^2}+\frac{\partial\theta_r}{r\partial r}-\left(1-\frac{D_{12}}{D_{11}}\right)\frac{\theta_r}{r^2}\right)-D_{11}c_1\left(\frac{\partial^3 w_0}{\partial r3}+\frac{\partial^2 w_0}{r\partial^2 r}-\left(1-\frac{D_{12}}{D_{11}}\right)\frac{\partial w_0}{r^2\partial r}\right)=I_0\ddot{u}_0+I_1\ddot{\theta}_r-I_3c_1\ddot{\theta}_r-I_3c_1\frac{\partial\ddot{w}_0}{\partial r},\\
&\delta\theta_r \Rightarrow\ B_{11}\left(\frac{\partial^2 u_0}{\partial r^2}+\frac{\partial u_0}{r\partial r}-\left(1-\frac{B_{12}}{B_{11}}\right)\frac{u_0}{r^2}\right)+E_{11}\left(\frac{\partial^2\theta_r}{\partial r^2}+\frac{\partial\theta_r}{r\partial r}-\left(1-\frac{E_{12}}{E_{11}}\right)\frac{\theta_r}{r^2}\right)-\\
&2c_1G_{11}\left(\frac{\partial^2\theta_r}{\partial r^2}+\frac{\partial\theta_r}{r\partial r}-\left(1-\frac{G_{12}}{G_{11}}\right)\frac{\theta_r}{r^2}\right)-c_1G_{11}\left(\frac{\partial^3 w_0}{\partial r^3}+\frac{\partial^2 w_0}{r\partial r^2}-\left(1-\frac{G_{12}}{G_{11}}\right)\frac{\partial w_0}{r^2\partial r}\right)\\
&+L_{31}\left(\frac{\partial\varphi}{\partial r}+\frac{\varphi}{r}\right)-D_{11}c_1\left(\frac{\partial^2 u_0}{\partial r^2}+\frac{\partial u_0}{r\partial r}-\left(1-\frac{D_{12}}{D_{11}}\right)\frac{u_0}{r^2}\right)+H_{11}c_1{}^2\left(\frac{\partial^2\theta_r}{\partial r^2}+\frac{\partial\theta_r}{r\partial r}-\left(1-\frac{H_{12}}{H_{11}}\right)\frac{\theta_r}{r^2}\right)+\\
&H_{11}c_1{}^2\left(\frac{\partial^3 w_0}{\partial r^3}+\frac{\partial^2 w_0}{r\partial r^2}-\left(1-\frac{H_{12}}{H_{11}}\right)\frac{\partial w_0}{r^2\partial r}\right)-c_1D_{13}\left(\frac{\partial\varphi}{\partial r}+\frac{\varphi}{r}\right)\\
&+\left(-A_{44}+3c_1B_{44}+3c_1E_{44}-9c_1{}^2D_{44}\right)\left(\theta_r+\frac{\partial w_0}{\partial r}\right)+M_{15}\left(\frac{\partial\varphi}{\partial r}+\frac{\varphi}{r}\right)\\
&-3c_1K_{15}\left(\frac{\partial\varphi}{\partial r}+\frac{\varphi}{r}\right)=I_1\ddot{u}_0+I_2\ddot{\theta}_r-I_3c_1\ddot{u}_0-2I_4c_1\ddot{\theta}_r+I_6c_1{}^2\ddot{\theta}_r-I_4c_1\frac{\partial\ddot{w}_0}{\partial r}+I_6c_1{}^2\frac{\partial\ddot{w}_0}{\partial r},\\
&\delta w_0 \Rightarrow\ c_1D_{11}\left(\frac{\partial^3 u_0}{\partial r^3}+2\frac{\partial^2 u_0}{r\partial r^2}-\left(1-2\frac{D_{12}}{D_{11}}\right)\frac{\partial u_0}{r^2\partial r}\right)+G_{11}c_1\left(\frac{\partial^3\theta_r}{\partial r^3}+2\frac{\partial^2\theta_r}{r\partial r^2}-\left(1-2\frac{G_{12}}{G_{11}}\right)\frac{\partial\theta_r}{r^2\partial r}\right)\\
&-H_{11}c_1{}^2\left(\frac{\partial^3\theta_r}{\partial r^3}+2\frac{\partial^2\theta_r}{r\partial r^2}-\left(1-2\frac{H_{12}}{H_{11}}\right)\frac{\partial\theta_r}{r^2\partial r}\right)-H_{11}c_1{}^2\left(\frac{\partial^4 w_0}{\partial r^4}+2\frac{\partial^3 w_0}{r\partial r^3}-\left(1-2\frac{H_{12}}{H_{11}}\right)\frac{\partial^2 w_0}{r^2\partial r^2}\right)+\\
&D_{13}c_1\left(\frac{\partial^2\varphi}{\partial r^2}+\frac{\partial\varphi}{r\partial r}\right)+\left(A_{44}-3c_1B_{44}-3c_1E_{44}+9c_1{}^2D_{44}\right)\left(\frac{\partial\theta_r}{\partial r}+\frac{\partial^2 w_0}{\partial r^2}+\frac{\theta_r}{r}+\frac{\partial w_0}{r\partial r}\right)\\
&-M_{15}\left(\frac{\partial^2\varphi}{\partial r^2}+\frac{\partial\varphi}{r\partial r}\right)+3c_1K_{15}\left(\frac{\partial^2\varphi}{\partial r^2}+\frac{\partial\varphi}{r\partial r}\right)+\left(N^P\right)\left(\frac{\partial^2 w_0}{\partial r^2}+\frac{\partial w_0}{r\partial r}\right)\\
&=q+I_0\ddot{w}_0+I_3c_1\frac{\partial\ddot{w}_0}{\partial r}+I_3c_1\frac{\ddot{u}_0}{r}+I_4c_1\frac{\partial\ddot{\theta}_r}{\partial r}+I_4c_1\frac{\ddot{\theta}_r}{r}-I_6c_1{}^2\frac{\partial\ddot{\theta}_r}{\partial r}-I_6c_1{}^2\frac{\ddot{\theta}_r}{r}-I_6c_1{}^2\frac{\partial^2\ddot{w}_0}{\partial r^2}-I_6c_1{}^2\frac{\partial\ddot{w}_0}{r\partial r},\\
&\delta\varphi \Rightarrow\ AA_1\left(\frac{\partial\theta_r}{\partial r}+\frac{\partial^2 w_0}{\partial r^2}\right)-3c_1AA_2\left(\frac{\partial\theta_r}{\partial r}+\frac{\partial^2 w_0}{\partial r^2}\right)+AA_3\left(\frac{\partial^2\varphi}{\partial r^2}+\frac{\partial\varphi}{r\partial r}\right)+AA_1\left(\frac{\theta_r}{r}+\frac{\partial w_0}{r\partial r}\right)\\
&-3c_1AA_2\left(\frac{\theta_r}{r}+\frac{\partial w_0}{r\partial r}\right)+AA_4\left(\frac{\partial\theta_r}{\partial r}+\frac{\theta_r}{r}\right)-3c_1AA_5\left(\frac{\partial\theta_r}{\partial r}+\frac{\partial^2 w_0}{\partial r^2}+\frac{\theta_r}{r}+\frac{\partial w_0}{r\partial r}\right)-AA_6\varphi=0
\end{aligned}
\tag{12}
$$

where the coefficients $A_{ij}$ , $B_{ij}$ , $D_{ij}$ , $E_{ij}$ , $G_{ij}$ , $H_{ij}$ , $K_{ij}$ , $M_{ij}$ , $L_{ij}$ and $AA_i$ are provided in Appendix B.

## 3 SOLUTION METHOD OF FG PIEZOELECTRIC SANDWICH ANNULAR PLATE

It should be noted that in the present work, the related boundary conditions at the inner and outer edges of the FGM piezoelectric sandwich annular plate supposed to be clamped or simply-suppoerted, which can be expressed as:

$$u_0=0,\ w_0=0,\ \frac{\partial w_0}{\partial r}=0,\ \theta_r=0,\ \varphi=0 \quad at \quad r=R_1,R_2 \tag{13}$$

For clamped boundary condition

$$u_0 = 0, w_0 = 0, M_{rr} = 0, P_{rr} = 0, \varphi = 0 \quad at \quad r = R_1, R_2 \tag{14}$$

For simply supported boundary condition.

In this section, to solve equilibrium equations, DQM is exerted for discretizing the governing equations and related boundary conditions. DQM is an efficient numerical method for solving the partial and ordinary differential equations. This technique states that a partial derivative of a function at a given discrete point can be estimated by a weighted linear combination of the functional values at all grid points. On the basis of the concept of DQM, derivative of any arbitrary function in arbitrary point can be rewritten in all intervals, and according to Chebyshev points, the grid points are computed as follows [36]

$$r_m = \frac{R_1}{R_2} + \frac{1-\dfrac{R_1}{R_2}}{2}\left(1-\cos\left(\frac{m-1}{n-1}\right)\pi\right), \quad m = 1,2,...,n. \tag{15}$$

where $n$ expresses the total number of nodes along the radial direction. Furthermore, *k-th* order differential operator is denoted as a finite series as:

$$\left.\frac{\partial^k \{u_0, w_0, \theta_r, \varphi\}}{\partial r^k}\right|_{r = r_i} = \sum_{m=1}^{n} C_{im}^{(k)} \{u_{0m}, w_{0m}, \theta_{rm}, \varphi_m\}, \quad i = 1,...,n \tag{16}$$

In which $C_{im}^{(k)}$ refers to the weighting coefficients for the *k-th* derivative [37]. By using DQM, the discretized form of the governing equations can be rewritten as:

$$[M]\ddot{x} + [K]x = F \tag{17}$$

where $[M]_{n\times n}$ and $[K]_{n\times n}$ are, respectively, the mass and stiffness matrices. Also, $\{x\}_{n\times 1}$ expresses modal displacements vector, which for obtaining time response, matrix form (17) is solved using Newmark-$\beta$ technique.

## 4 NUMERICAL RESULTS AND DISCUSSION

### *4.1 Convergence checking*

In this section, the convergence checking of computations is systematically is ensured in a standard trial & error manner, i.e., by accumulating the number of nodes distributed along the radial direction of FGM piezoelectric sandwich clamped annular plate, $n$, while looking for stability in the predicted natural frequency and time response. Hence, by dropping the external forces, the results depicted in Fig. 2 indicate the convergence of the calculated four first natural frequencies. As shown, at least 15 nodes ($n$=15) are required for proper convergence of numerical solutions. Here, initial external electric potential ($V$) is assumed to be zero, and $R_1 = 0.3m$, $R_2 = 1m$, $K = 1$, $h_e = 0.001m$, $h_p = 0.005m$ . In addition, material and physical parameters used for FGM and piezoelectric material in this section and the following sections (except for verification of results section) are listed in Table 1 and Table 2.

**Table 1**
Material properties of FGM core plate.

| Properties | Al | Si |
|---|---|---|
| Young's modulus $E$ ($GPa$) | 70 | 210 |
| Mass density $\rho\left(\frac{kg}{m^3}\right)$ | 2700 | 2331 |

**Table 2**
Material properties of PZT-4 piezoelectric.

| Properties | PZT4 |
|---|---|
| $C_{11}\,(GPa)$ | 139 |
| $C_{12}\,(GPa)$ | 77.8 |
| $C_{13}\,(GPa)$ | 74 |
| $C_{22}\,(GPa)$ | 77.8 |
| $C_{23}\,(GPa)$ | 74 |
| $C_{33}\,(GPa)$ | 115 |
| $C_{44}\,(GPa)$ | 25.6 |
| $C_{55}\,(GPa)$ | 25.6 |
| $C_{66}\,(GPa)$ | 30.6 |
| $e_{15}\left(C/m^2\right)$ | 12.7 |
| $e_{24}\left(C/m^2\right)$ | 12.7 |
| $e_{31}\left(C/m^2\right)$ | -5.2 |
| $e_{32}\left(C/m^2\right)$ | -5.2 |
| $e_{33}\left(C/m^2\right)$ | 15.1 |
| $k_{11}\left(10^{-9}F/m\right)$ | 6.46 |
| $k_{22}\left(10^{-9}F/m\right)$ | 6.46 |
| $k_{33}\left(10^{-9}F/m\right)$ | 5.62 |
| $\rho\left(kg/m^3\right)$ | 7500 |

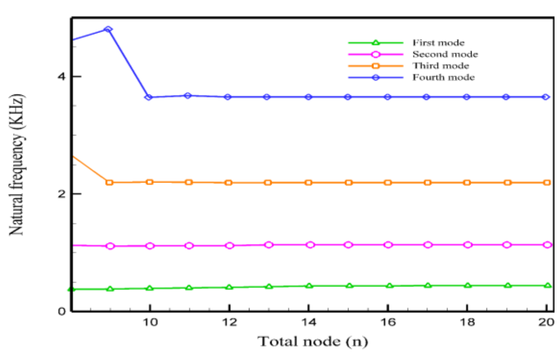


**Fig.2**
The four first natural frequency (*KHz*) of FGM piezoelectric sandwich plate with varying total number of nodes.

*4.2 Comparison study*

To show the correctness and validity of the achieved formulation, firstly, by ignoring piezoelectric layers, the two first dimensionless frequencies ( $\lambda = \omega R_o^2\sqrt{\frac{\rho h}{D}},\ D = \frac{Eh^3}{12\left(1-\upsilon^2\right)}$ ) are calculated and listed in Table 3., along with numerical measurements were presented previously by Ref. [38] for clamped boundary conditions. It is essential to reminder that in Ref. [38] FSDT is assumed for deflection field and equilibrium equations are solved by the *p*-version Ritz method. Based upon Table 3, it can be showed that the calculated results are in good agreement with the results of Ref.[38].

**Table 3**
Comparison study of the two first non-dimensional natural frequencies of FGM annular plate.

| $\varphi = \frac{R_i}{R_o}$ | Method | 0.1 | 0.3 | 0.5 |
|---|---|---|---|---|
| $\lambda_1$ | Present (DQM) | 19.65261 | 30.79739 | 52.51617 |
| | Liew et al.[38](Ritz) | 19.84 | 30.04 | 48.31 |
| $\lambda_2$ | Present (DQM) | 46.88275 | 69.89355 | 113.9494 |
| | Liew et al.[38](Ritz) | 44.91 | 64.23 | 97.39 |

In another verification investigation, a comparison between three first natural frequencies obtained for FGM piezoelectric sandwich annular plate against different material gradient parameters with those obtained by [39] is indicated in Table 4. By briefly reviewing the computed results in this table, the accuracy of present formulations will be determined.

**Table 4**
Comparison study of the natural frequencies (Hz) of FGM piezoelectric sandwich annular plate $R_2/h = 60$.

| Material gradient index | Mode number | Ebrahimi and Rastgoo [39] | Present |
|---|---|---|---|
| | First | 448.39 | 449.11 |
| 0 | Second | 1238.35 | 1240.46 |
| | Third | 2433.48 | 2436.38 |
| | First | 435.37 | 436.42 |
| 1 | Second | 1205.80 | 1208.03 |
| | Third | 2371.07 | 2376.75 |

*4.3 Benchmark results*

In this section, natural frequencies and time response of FGM piezoelectric sandwich annular plate with are numerically for both boundary conditions computed and discussed in detail.

*4.4 Free vibration*

In order to obtain the natural frequencies of the system, modal displacements vector must be equal to $\{x\}_{n\times 1} = \{X\}_{n\times 1} e^{i\omega t}$ and external force must be equal to zero. Here, $\omega$ expresses the natural frequency and $\{X\}_{n\times 1}$ is modal coefficient vector.

Depicted in Fig. 3 is the effect of inner-to-outer radius ratio on the variations of the four first natural frequencies plots of FG piezoelectric sandwich plate under clamped (for inner and outer boundaries) and simply supported boundary conditions (for inner and outer boundaries). Here, initial external electric potential ($V$) is assumed to be zero, and $K = 1$, $h_e = 0.001m$, $h_p = 0.005m$ . As figure illustrates, Because of the stiffness-hardening effect of inner-to-outer radius ratio on the plate mode, natural frequency increases by increasing inner-to-outer radius ratio. Furthermore, because of the high stiffness of clamped boundary condition, the clamped boundary condition has higher frequency than that of simply supported boundary condition.

Fig. 4 reveals the effect of the material gradient index on the variations of the four first natural frequencies plots of FG piezoelectric sandwich plate. Here, external electric voltage ($V$) is supposed to be zero, and $R_1 = 0.3m$, $R_2 = 1m$, $h_e = 0.001m$, $h_p = 0.005m$ . It should be pointed out by increasing power law model index ($K$), the material characteristics of FG core annular plate shift continuously and smoothly from a fully metal part at the top plane to a fully ceramic part at the bottom plane. It is generally concluded from this figure that by increasing material gradient, the total stiffness of the system raises and consequently the natural frequency increases.

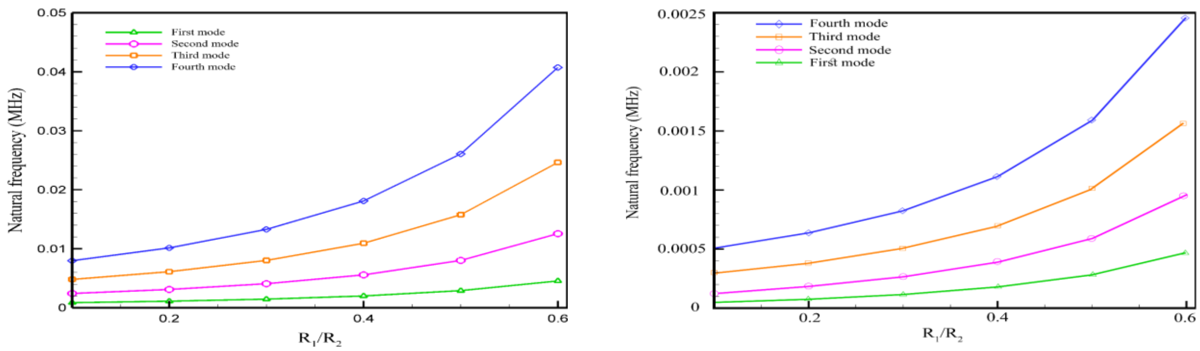


(a) (b)

**Fig.3**
a) The effect of inner-to-outer radius ratio on the variations of the natural frequency for clamped boundary condition. b) The effect of inner-to-outer radius ratio on the variations of the natural frequency for simply supported boundary condition.

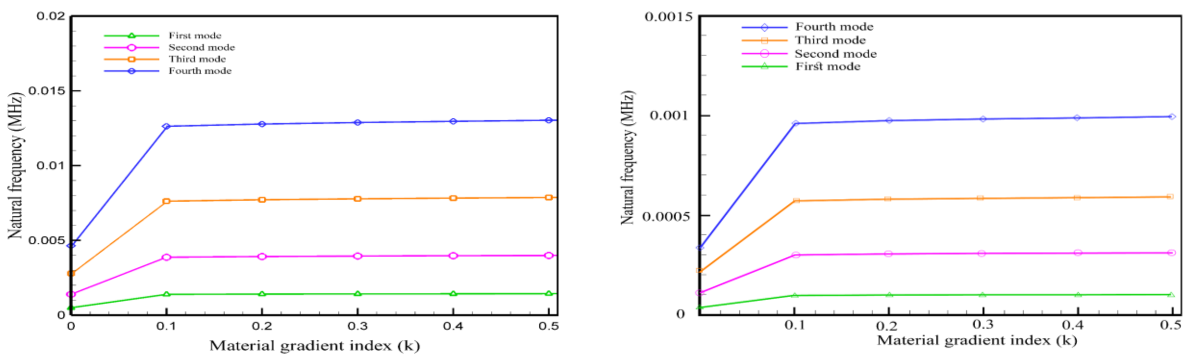


(a) (b)

**Fig.4**
a) The effect of material gradient parameter on the changes of the natural frequency for clamped boundary condition.
b)The effect of material gradient parameter on the changes of the natural frequency for simply supported boundary condition.

The influence of the external electric voltage on the variations of the four first natural frequencies of FGM piezoelectric sandwich annular plate is represented in Fig. 5. Here, $R_1 = 0.3m$, $R_2 = 1m$, $K = 1, h_e = 0.001m$, $h_p = 0.005m$ .

The most interesting result is the fact that increasing the value of external electric voltage from 100 $V$ to 200 $V$, the natural frequency reduces.

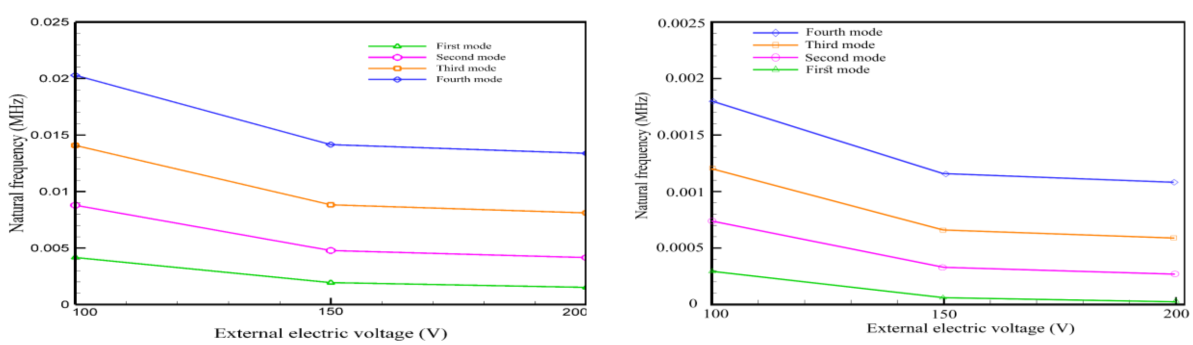


(a) (b)

**Fig.5**
a) The effect of initial external electric voltage on the changes of the natural frequency for clamped boundary condition. b) The effect of initial external electric voltage on the changes of the natural frequency for simply supported boundary condition.

*4.5 Time response*

In this section the time response of FGM piezoelectric sandwich annular plate under a simple harmonic excitation $q = q_0 r^2 \sin 2t$ is performed. Here, $q_0$ refers to the constant load.

Fig. 6 displays the influence of the inner-to-outer radius ratio on the changes of the time response at a chosen location $\left\{ r_{av} = {(R_1 + R_2)}/{2} \right\}$ over the time range of 0-10 *s*. Here, initial external electric potential (*V*) is assumed to be zero, and $K = 1$, $h_e = 0.001m$, $h_p = 0.005m$ . It is obvious that by increasing inner-to-outer radius ratio, the stiffness-hardening effect of the system reduces the peak deflection.

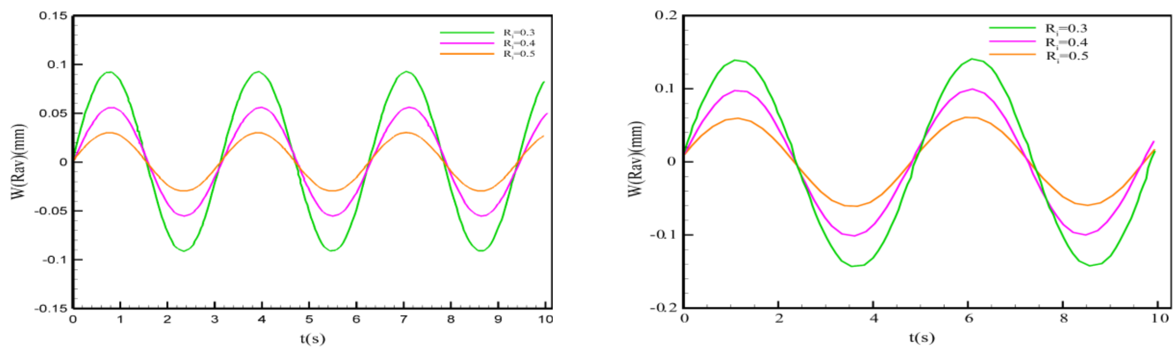


(a) (b)

**Fig.6**
a) The effect of inner-to-outer radius ratio on the dynamic behavior of FGM piezoelectric sandwich annular plate under sinusoidal loading for clamped boundary condition.
b) The effect of inner-to-outer radius ratio on the dynamic behavior of FGM piezoelectric sandwich annular plate under sinusoidal loading for clamped boundary condition.

In order to investigate the effect of the material gradient index on the behavior of dynamic deflection of FGM piezoelectric sandwich annular plate, Fig. 7 is presented. Here, initial external electric potential (*V*) is assumed to be zero, and $R_1 = 0.3m$, $R_2 = 1m$, $h_e = 0.001m$, $h_p = 0.005m$ . It can be seen that the by increasing material gradient index, the vibration amplitude will be decreased.

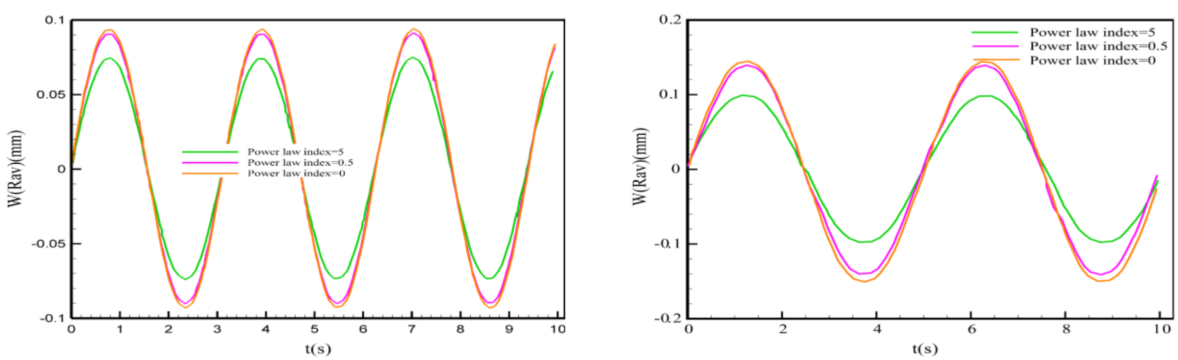


(a) (b)

**Fig.7**
a) The effect of the material gradient index on the dynamic behavior of FGM piezoelectric sandwich annular plate under sinusoidal loading for clamped boundary condition. b) The effect of the material gradient index on the dynamic behavior of FGM piezoelectric sandwich annular plate under sinusoidal loading for simply supported boundary condition.

Fig. 8 shows the effect of FGM core thickness on the variations of the time response of FGM piezoelectric sandwich annular plate over the time range of $0-10s$ . Here, initial external electric potential (*V*) is assumed to be zero, and $R_1 = 0.3m$, $R_2 = 1m$, $K = 1$, $h_p = 0.005m$ . As it may be readily seen, by increasing FGM core thickness, the amplitude increases.

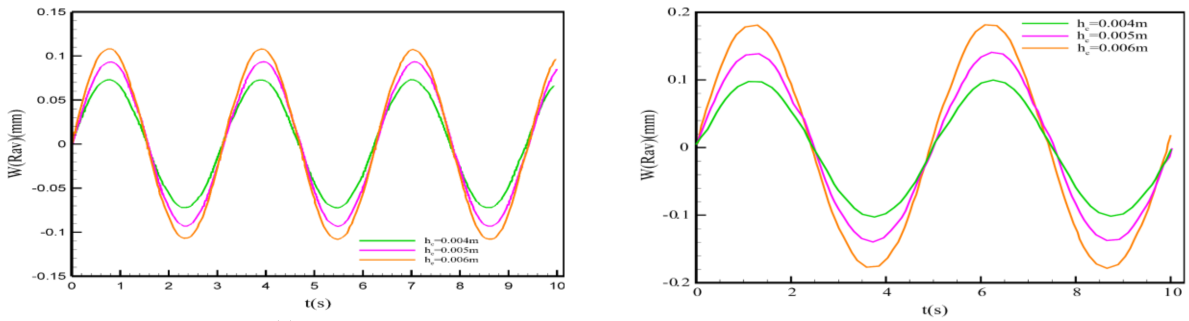


(a) (b)

**Fig.8**
a) The effect of FGM core thickness on the dynamic behavior of FGM piezoelectric sandwich annular plate under sinusoidal loading for clamped boundary condition. b) The effect of FGM core thickness on the dynamic behavior of FGM piezoelectric sandwich annular plate under sinusoidal loading for simply supported boundary condition.

Finally, Fig. 9 demonstrates the effect of initial external electric voltage on the changes of the dynamic response of FGM piezoelectric sandwich plate under sinusoidal loading. Here, $R_1 = 0.3m$, $R_2 = 1m$, $K = 1$, $h_e = 0.001m$, $h_p = 0.005m$ . The most interesting result is the fact that an increase in the value of the electric voltage reduces the vibration amplitude and controls the dynamic response.

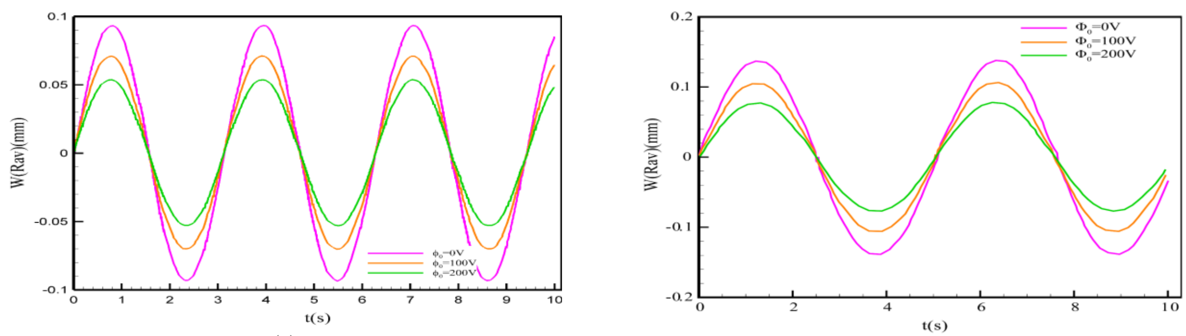


(a) (b)

**Fig.9**
a) The effect of initial electric voltage on the dynamic behavior of FGM piezoelectric sandwich annular plate under sinusoidal loading for clamped boundary condition. b) The effect of initial electric voltage on the dynamic behavior of FGM piezoelectric sandwich annular plate under sinusoidal loading for simply supported boundary condition.

## 5 CONCLUSIONS

A numerical model was exhibited to analyze the behavior of free vibration and transient response of FGM piezoelectric sandwich annular plate with piezoelectric layers and FGM core. By using the power law distribution model, the impressive material properties of FGM core plate shift smoothly in the plate thickness. Governing partial formulations obtained by employing Hamilton's method, then differential quadrature method (DQM) in conjunction with Newmark-β was implemented to solve equilibrium equations. Finally, numerical results were exhibited to show how to change the natural frequency and dynamic response by varying the external electric voltage, material gradient, FGM core thickness, and inner-to-outer radius ratio. The major results are sum up as follows:

- The natural frequency increases by increasing inner-to-outer radius ratio.
- By increasing power law index, the total stiffness of the system increases and accordingly the natural frequency rises.

- An increase in the value of external electric voltage reduces the natural frequency.
- The electric voltage reduces the vibration amplitude and controls the dynamic response.
- By increasing inner-to-outer radius ratio, the stiffness-hardening effect of the system reduces the peak deflection.

**APPENDIX A**

$$\begin{aligned}\delta U = &\iint_S \int_{-\frac{h_e}{2}-h_p}^{-\frac{h_e}{2}} (\sigma_{rr}^p \delta\varepsilon_{rr}^p + \sigma_{\theta\theta}^p \delta\varepsilon_{\theta\theta}^p + \sigma_{rz}^p \delta\gamma_{rz}^p - D_r^p \delta E_r^p - D_z^p \delta E_z^p) dz dS + \\ &\iint_S \int_{-\frac{h_e}{2}}^{\frac{h_e}{2}} (\sigma_{rr}^e \delta\varepsilon_{rr}^e + \sigma_{\theta\theta}^e \delta\varepsilon_{\theta\theta}^e + \sigma_{rz}^e \delta\gamma_{rz}^e) dz dS + \\ &\iint_S \int_{\frac{h_e}{2}}^{\frac{h_e}{2}+h_p} (\sigma_{rr}^p \delta\varepsilon_{rr}^p + \sigma_{\theta\theta}^p \delta\varepsilon_{\theta\theta}^p + \sigma_{rz}^p \delta\gamma_{rz}^p - D_r^p \delta E_r^p - D_z^p \delta E_z^p) dz dS\end{aligned} \tag{A.1}$$

$$\begin{aligned}\delta T = &\iint_S \int_{-\frac{h_e}{2}-h_p}^{-\frac{h_e}{2}} \Big[ \rho^p (\dot{u}_0 \delta\dot{u}_0 + \dot{w}_0 \delta\dot{w}_0) - \rho^p z^4 \frac{4}{3h^2} (2\dot{\theta}_r \delta\dot{\theta}_r + \dot{\theta}_r \partial \frac{\delta\dot{w}_0}{\partial r} + \delta\dot{\theta}_r \frac{\partial\dot{w}_0}{\partial r}) \\ &\quad - \rho^p z^3 \frac{4}{3h^2} (\dot{u}_0 \delta\dot{\theta}_r + \dot{u}_0 \partial \frac{\delta\dot{w}_0}{\partial r} + \dot{\theta}_r \delta\dot{u}_0 + \delta\dot{u}_0 \frac{\partial\dot{w}_0}{\partial r}) \\ &\quad + \rho^p z (\dot{u}_0 \delta\dot{\theta}_r + \dot{\theta}_r \delta\dot{u}_0) + \rho^p z^2 \dot{\theta}_r \delta\dot{\theta}_r \\ &\quad - \rho^p z^6 (\frac{4}{3h^2})^2 (\dot{\theta}_r \delta\dot{\theta}_r + \dot{\theta}_r \partial \frac{\delta\dot{w}_0}{\partial r} + \delta\dot{\theta}_r \frac{\partial\dot{w}_0}{\partial r} + \frac{\partial\dot{w}_0}{\partial r} \delta \frac{\partial\dot{w}_0}{\partial r}) \Big] dz dS \\ &+ \iint_S \int_{-\frac{h_e}{2}}^{\frac{h_e}{2}} \Big[ \rho^e (\dot{u}_0 \delta\dot{u}_0 + \dot{w}_0 \delta\dot{w}_0) - \rho^e z^4 \frac{4}{3h^2} (2\dot{\theta}_r \delta\dot{\theta}_r + \dot{\theta}_r \partial \frac{\delta\dot{w}_0}{\partial r} + \delta\dot{\theta}_r \frac{\partial\dot{w}_0}{\partial r}) \\ &\quad - \rho^e z^3 \frac{4}{3h^2} (\dot{u}_0 \delta\dot{\theta}_r + \dot{u}_0 \partial \frac{\delta\dot{w}_0}{\partial r} + \dot{\theta}_r \delta\dot{u}_0 + \delta\dot{u}_0 \frac{\partial\dot{w}_0}{\partial r}) \\ &\quad + \rho^e z (\dot{u}_0 \delta\dot{\theta}_r + \dot{\theta}_r \delta\dot{u}_0) + \rho^p z^2 \dot{\theta}_r \delta\dot{\theta}_r \\ &\quad - \rho^e z^6 (\frac{4}{3h^2})^2 (\dot{\theta}_r \delta\dot{\theta}_r + \dot{\theta}_r \partial \frac{\delta\dot{w}_0}{\partial r} + \delta\dot{\theta}_r \frac{\partial\dot{w}_0}{\partial r} + \frac{\partial\dot{w}_0}{\partial r} \delta \frac{\partial\dot{w}_0}{\partial r}) \Big] dz dS \\ &+ \iint_S \int_{\frac{h_e}{2}}^{\frac{h_e}{2}+h_p} \Big[ \rho^p (\dot{u}_0 \delta\dot{u}_0 + \dot{w}_0 \delta\dot{w}_0) - \rho^p z^4 \frac{4}{3h^2} (2\dot{\theta}_r \delta\dot{\theta}_r + \dot{\theta}_r \partial \frac{\delta\dot{w}_0}{\partial r} + \delta\dot{\theta}_r \frac{\partial\dot{w}_0}{\partial r}) \\ &\quad - \rho^p z^3 \frac{4}{3h^2} (\dot{u}_0 \delta\dot{\theta}_r + \dot{u}_0 \partial \frac{\delta\dot{w}_0}{\partial r} + \dot{\theta}_r \delta\dot{u}_0 + \delta\dot{u}_0 \frac{\partial\dot{w}_0}{\partial r}) \\ &\quad + \rho^p z (\dot{u}_0 \delta\dot{\theta}_r + \dot{\theta}_r \delta\dot{u}_0) + \rho^p z^2 \dot{\theta}_r \delta\dot{\theta}_r \\ &\quad - \rho^p z^6 (\frac{4}{3h^2})^2 (\dot{\theta}_r \delta\dot{\theta}_r + \dot{\theta}_r \partial \frac{\delta\dot{w}_0}{\partial r} + \delta\dot{\theta}_r \frac{\partial\dot{w}_0}{\partial r} + \frac{\partial\dot{w}_0}{\partial r} \delta \frac{\partial\dot{w}_0}{\partial r}) \Big] dz dS\end{aligned} \tag{A.2}$$

$$\delta W_{ext} = \int_S \left\{ \left(N^P\right) \left( \frac{\partial w_0}{\partial r} \frac{\delta\partial w_0}{\partial r} \right) + q\,\delta w_0 \right\} dS \tag{A.3}$$

where term $\left(N^P\right)$ expresses the normal force caused by initial external electric, and can be denoted as:

$$N^P = 2 \left\{ \int_{-\frac{h_e}{2}-h_p}^{-\frac{h_e}{2}} \bar{e}_{31} V \big/ h_p \, dz + \int_{\frac{h_e}{2}}^{\frac{h_e}{2}+h_p} \bar{e}_{31} V \big/ h_p \, dz \right\} \tag{A.4}$$

In order to achieve the governing equation of motion using Hamilton's principle, virtual strain energy variation (Eq. (A.1)) could be rewritten as:

$$
\begin{aligned}
&\int_S\int_{-\frac{h_e}{2}-h_p}^{-\frac{h_e}{2}} \sigma_{rr}^p \delta\varepsilon_{rr}^p = \int_S (N_{rr}^A \partial\frac{\delta u_0}{\partial r} + M_{rr}^A \partial\frac{\delta\theta_r}{\partial r} - c_1 P_{rr}^A (\partial\frac{\delta\theta_r}{\partial r} + \partial^2\frac{\delta w_0}{\partial r^2}))dS \ , \\
&\int_S\int_{-\frac{h_e}{2}-h_p}^{-\frac{h_e}{2}} \sigma_{\theta\theta}^p \delta\varepsilon_{\theta\theta}^p = \int_S (N_{\theta\theta}^A \frac{\delta u_0}{r} + M_{\theta\theta}^A \frac{\delta\theta_r}{r} - c_1 P_{\theta\theta}^A (\delta\theta_r + \partial\frac{\delta w_0}{\partial r}))dS \ , \\
&\int_S\int_{-\frac{h_e}{2}-h_p}^{-\frac{h_e}{2}} \sigma_{rz}^p \delta\gamma_{rz}^p = \int_S (Q_{rz}^A (\delta\theta_r + \partial\frac{\delta w_0}{\partial r}) - 3c_1 R_{rz}^A (\delta\theta_r + \partial\frac{\delta w_0}{\partial r}))dS \ , \\
&\int_S\int_{-\frac{h_e}{2}-h_p}^{-\frac{h_e}{2}} D_r^p \delta E_r^p dzdS = \int_S\int_{-\frac{h_e}{2}-h_p}^{-\frac{h_e}{2}} (D_r^p \cos(\pi\frac{2-\frac{h_e}{2}-\frac{h_p}{2}}{h_p})\partial\frac{\delta\phi}{\partial r})dzdS \ , \\
&\int_S\int_{-\frac{h_e}{2}-h_p}^{-\frac{h_e}{2}} D_z^p \delta E_z^p dzdS = \int_S\int_{-\frac{h_e}{2}-h_p}^{-\frac{h_e}{2}} (D_z^p \frac{\pi}{h_m}\sin(\pi\frac{2-\frac{h_e}{2}-\frac{h_p}{2}}{h_p})\delta\phi)dzdS \ , \\
&\int_S\int_{-\frac{h_e}{2}}^{\frac{h_e}{2}} \sigma_{rr}^e \delta\varepsilon_{rr}^e = \int_S (N_{rr}^B \partial\frac{\delta u_0}{\partial r} + M_{rr}^B \partial\frac{\delta\theta_r}{\partial r} - c_1 P_{rr}^B (\partial\frac{\delta\theta_r}{\partial r} + \partial^2\frac{\delta w_0}{\partial r^2}))dS \ , \\
&\int_S\int_{-\frac{h_e}{2}}^{\frac{h_e}{2}} \sigma_{\theta\theta}^e \delta\varepsilon_{\theta\theta}^e = \int_S (N_{\theta\theta}^B \frac{\delta u_0}{r} + M_{\theta\theta}^B \frac{\delta\theta_r}{r} - c_1 P_{\theta\theta}^B (\delta\theta_r + \partial\frac{\delta w_0}{\partial r}))dS \ , \\
&\int_S\int_{-\frac{h_e}{2}}^{\frac{h_e}{2}} \sigma_{rz}^e \delta\gamma_{rz}^e = \int_S (Q_{rz}^B (\delta\theta_r + \partial\frac{\delta w_0}{\partial r}) - 3c_1 R_{rz}^B (\delta\theta_r + \partial\frac{\delta w_0}{\partial r}))dS \ , \\
&\int_S\int_{\frac{h_e}{2}}^{\frac{h_e}{2}+h_p} \sigma_{rr}^p \delta\varepsilon_{rr}^p = \int_S (N_{rr}^C \partial\frac{\delta u_0}{\partial r} + M_{rr}^C \partial\frac{\delta\theta_r}{\partial r} - c_1 P_{rr}^C (\partial\frac{\delta\theta_r}{\partial r} + \partial^2\frac{\delta w_0}{\partial r^2}))dS \ , \\
&\int_S\int_{\frac{h_e}{2}}^{\frac{h_e}{2}+h_p} \sigma_{\theta\theta}^p \delta\varepsilon_{\theta\theta}^p = \int_S (N_{\theta\theta}^C \frac{\delta u_0}{r} + M_{\theta\theta}^C \frac{\delta\theta_r}{r} - c_1 P_{\theta\theta}^C (\delta\theta_r + \partial\frac{\delta w_0}{\partial r}))dS \ , \\
&\int_S\int_{\frac{h_e}{2}}^{\frac{h_e}{2}+h_p} \sigma_{rz}^p \delta\gamma_{rz}^p = \int_S (Q_{rz}^C (\delta\theta_r + \partial\frac{\delta w_0}{\partial r}) - 3c_1 R_{rz}^C (\delta\theta_r + \partial\frac{\delta w_0}{\partial r}))dS \\
&\int_S\int_{\frac{h_e}{2}}^{\frac{h_e}{2}+h_p} D_r^p \delta E_r^p dzdS = \int_S\int_{\frac{h_e}{2}}^{\frac{h_e}{2}+h_p} (D_r^p \cos(\pi\frac{z-\frac{h_e}{2}-\frac{h_p}{2}}{h_p})\partial\frac{\delta\phi}{\partial r})dzdS \ , \\
&\int_S\int_{\frac{h_e}{2}}^{\frac{h_e}{2}+h_p} D_z^p \delta E_z^p dzdS = \int_S\int_{\frac{h_e}{2}}^{\frac{h_e}{2}+h_p} (-D_z \frac{\pi}{h_m}\sin(\pi\frac{z-\frac{h_e}{2}-\frac{h_p}{2}}{h_p})\delta\phi)dzdS
\end{aligned}
\tag{A.5}
$$

In which $c_1 = \dfrac{4}{3\left(\dfrac{h_e}{2}+h_p\right)^2}$ and in which *S* indicates the area of the mid-plane of sandwich plate. Also, it should be noted that superscripts *A, B* and *C* refer to, respectively, upper piezoelectric face sheet, FGM core, and bottom piezoelectric face sheet. Furthermore, terms $N_{ij}$, $M_{ij}$, $P_{ij}$, $Q_{rz}$ and $R_{rz}$ are demonstrated as follows:

$$
\begin{aligned}
N_{rr}^A &= \int_{-\frac{h_e}{2}-h_p}^{-\frac{h_e}{2}} \sigma_{rr}^p dz = \int_{-\frac{h_e}{2}-h_p}^{-\frac{h_e}{2}} \Big[\bar{c}_{11}(\frac{\partial u_0}{\partial r} + z\frac{\partial\theta_r}{\partial r} - \frac{4z^3}{3h^2}(\frac{\partial\theta_r}{\partial r} + \frac{\partial^2 w}{\partial r^2})) \\
&\quad + \bar{c}_{12}(\frac{u_0}{r} + \frac{z\,\theta_r}{r} - \frac{4z^3}{3h^2 r}(\theta_r + \frac{\partial w}{\partial r})) - \bar{e}_{31}E_z\Big]dz \ ,
\end{aligned}
\tag{A.6}
$$

$$
\begin{aligned}
M_{rr}^{A} &= \int_{-\frac{h_e}{2}-h_p}^{-\frac{h_e}{2}} \sigma_{rr}^{p} z dz = \int_{-\frac{h_e}{2}-h_p}^{-\frac{h_e}{2}} \Big[\bar{c}_{11} z \Big(\frac{\partial u_0}{\partial r} + z\frac{\partial \theta_r}{\partial r} - \frac{4z^3}{3h^2}\Big(\frac{\partial \theta_r}{\partial r} + \frac{\partial^2 w}{\partial r^2}\Big)\Big) \\
&\quad + \bar{c}_{12} z \Big(\frac{u_0}{r} + \frac{z\,\theta_r}{r} - \frac{4z^3}{3h^2 r}\Big(\theta_r + \frac{\partial w}{\partial r}\Big)\Big) - \bar{e}_{31} z E_z\Big] dz \ , \\
P_{rr}^{A} &= \int_{-\frac{h_e}{2}-h_p}^{-\frac{h_e}{2}} \sigma_{rr}^{p} z^3 dz = \int_{-\frac{h_e}{2}-h_p}^{-\frac{h_e}{2}} \Big[\bar{c}_{11} z^3 \Big(\frac{\partial u_0}{\partial r} + z\frac{\partial \theta_r}{\partial r} - \frac{4z^3}{3h^2}\Big(\frac{\partial \theta_r}{\partial r} + \frac{\partial^2 w}{\partial r^2}\Big)\Big) \\
&\quad + \bar{c}_{12} z^3 \Big(\frac{u_0}{r} + \frac{z\,\theta_r}{r} - \frac{4z^3}{3h^2 r}\Big(\theta_r + \frac{\partial w}{\partial r}\Big)\Big) - \bar{e}_{31} z^3 E_z\Big] dz \\
N_{\theta\theta}^{A} &= \int_{-\frac{h_e}{2}-h_p}^{-\frac{h_e}{2}} \sigma_{\theta\theta}^{p} dz = \int_{-\frac{h_e}{2}-h_p}^{-\frac{h_e}{2}} \Big[\bar{c}_{21} \Big(\frac{\partial u_0}{\partial r} + z\frac{\partial \theta_r}{\partial r} - \frac{4z^3}{3h^2}\Big(\frac{\partial \theta_r}{\partial r} + \frac{\partial^2 w}{\partial r^2}\Big)\Big) \\
&\quad + \bar{c}_{22} \Big(\frac{u_0}{r} + \frac{z\,\theta_r}{r} - \frac{4z^3}{3h^2 r}\Big(\theta_r + \frac{\partial w}{\partial r}\Big)\Big) - \bar{e}_{32} E_z\Big] dz \ , \\
M_{\theta\theta}^{A} &= \int_{-\frac{h_e}{2}-h_p}^{-\frac{h_e}{2}} \sigma_{\theta\theta}^{p} z dz = \int_{-\frac{h_e}{2}-h_p}^{-\frac{h_e}{2}} \Big[\bar{c}_{21} z \Big(\frac{\partial u_0}{\partial r} + z\frac{\partial \theta_r}{\partial r} - \frac{4z^3}{3h^2}\Big(\frac{\partial \theta_r}{\partial r} + \frac{\partial^2 w}{\partial r^2}\Big)\Big) \\
&\quad + \bar{c}_{22} z \Big(\frac{u_0}{r} + \frac{z\,\theta_r}{r} - \frac{4z^3}{3h^2 r}\Big(\theta_r + \frac{\partial w}{\partial r}\Big)\Big) - \bar{e}_{32} z E_z\Big] dz \ , \\
P_{\theta\theta}^{A} &= \int_{-\frac{h_e}{2}-h_p}^{-\frac{h_e}{2}} \sigma_{rr}^{p} z^3 dz = \int_{-\frac{h_e}{2}-h_p}^{-\frac{h_e}{2}} \Big[\bar{c}_{21} z^3 \Big(\frac{\partial u_0}{\partial r} + z\frac{\partial \theta_r}{\partial r} - \frac{4z^3}{3h^2}\Big(\frac{\partial \theta_r}{\partial r} + \frac{\partial^2 w}{\partial r^2}\Big)\Big) \\
&\quad + \bar{c}_{22} z^3 \Big(\frac{u_0}{r} + \frac{z\,\theta_r}{r} - \frac{4z^3}{3h^2 r}\Big(\theta_r + \frac{\partial w}{\partial r}\Big)\Big) - \bar{e}_{32} z^3 E_z\Big] dz \\
Q_{rz}^{A} &= \int_{-\frac{h_e}{2}-h_p}^{-\frac{h_e}{2}} \sigma_{rz}^{p} dz = \int_{-\frac{h_e}{2}-h_p}^{-\frac{h_e}{2}} \Big(\bar{c}_{44}\Big(1 - \frac{4z}{h^2}\Big)\Big(\theta_r + \frac{\partial w}{\partial r}\Big) - \bar{e}_{15} E_r\Big) dz \ , \\
R_{rz}^{A} &= \int_{-\frac{h_e}{2}-h_p}^{-\frac{h_e}{2}} \sigma_{rz}^{p} z^2 dz = \int_{-\frac{h_e}{2}-h_p}^{-\frac{h_e}{2}} \Big(\bar{c}_{44} z^2\Big(1 - \frac{4z}{h^2}\Big)\Big(\theta_r + \frac{\partial w}{\partial r}\Big) - \bar{e}_{15} z^2 E_r\Big) dz \\
N_{rr}^{B} &= \int_{-\frac{h_e}{2}}^{\frac{h_e}{2}} \sigma_{rr}^{e} dz = \int_{-\frac{h_e}{2}}^{\frac{h_e}{2}} \frac{E(z)}{1-\nu^2}\Big[\Big(\frac{\partial u_0}{\partial r} + z\frac{\partial \theta_r}{\partial r} - \frac{4z^3}{3h^2}\Big(\frac{\partial \theta_r}{\partial r} + \frac{\partial^2 w}{\partial r^2}\Big)\Big) \\
&\quad + \frac{\nu E(z)}{1-\nu^2}\Big(\frac{u_0}{r} + \frac{z\,\theta_r}{r} - \frac{4z^3}{3h^2 r}\Big(\theta_r + \frac{\partial w}{\partial r}\Big)\Big) dz \ , \\
M_{rr}^{B} &= \int_{-\frac{h_e}{2}}^{\frac{h_e}{2}} \sigma_{rr}^{e} z dz = \int_{-\frac{h_e}{2}}^{\frac{h_e}{2}} \frac{zE(z)}{1-\nu^2}\Big[\Big(\frac{\partial u_0}{\partial r} + z\frac{\partial \theta_r}{\partial r} - \frac{4z^3}{3h^2}\Big(\frac{\partial \theta_r}{\partial r} + \frac{\partial^2 w}{\partial r^2}\Big)\Big) dz \\
&\quad + \frac{\nu z E(z)}{1-\nu^2}\Big(\frac{u_0}{r} + \frac{z\,\theta_r}{r} - \frac{4z^3}{3h^2 r}\Big(\theta_r + \frac{\partial w}{\partial r}\Big)\Big) dz \ , \\
P_{rr}^{B} &= \int_{-\frac{h_e}{2}}^{\frac{h_e}{2}} \sigma_{rr}^{e} z^3 dz = \int_{-\frac{h_e}{2}}^{\frac{h_e}{2}} \frac{z^3 E(z)}{1-\nu^2}\Big[\Big(\frac{\partial u_0}{\partial r} + z\frac{\partial \theta_r}{\partial r} - \frac{4z^3}{3h^2}\Big(\frac{\partial \theta_r}{\partial r} + \frac{\partial^2 w}{\partial r^2}\Big)\Big) dz \\
&\quad + \frac{\nu z^3 E(z)}{1-\nu^2}\Big(\frac{u_0}{r} + \frac{z\,\theta_r}{r} - \frac{4z^3}{3h^2 r}\Big(\theta_r + \frac{\partial w}{\partial r}\Big)\Big) dz \\
Q_{rz}^{B} &= \int_{-\frac{h_e}{2}}^{\frac{h_e}{2}} \sigma_{rz} dz = \int_{-\frac{h_e}{2}}^{\frac{h_e}{2}} \frac{E(z)}{2(1+\nu)}\Big(1 - \frac{4z}{h^2}\Big)\Big(\theta_r + \frac{\partial w}{\partial r}\Big) dz \ , \\
R_{rz}^{B} &= \int_{-\frac{h_e}{2}}^{\frac{h_e}{2}} \sigma_{rz} z^2 dz = \int_{-\frac{h_e}{2}}^{\frac{h_e}{2}} \frac{z^2 E(z)}{2(1+\nu)}\Big(1 - \frac{4z}{h^2}\Big)\Big(\theta_r + \frac{\partial w}{\partial r}\Big) dz
\end{aligned}
\tag{A.6}
$$

$$
\begin{aligned}
N_{\theta\theta}^{B} &= \int_{-\frac{h_e}{2}}^{\frac{h_e}{2}} \sigma_{\theta\theta}^{e} dz = \int_{-\frac{h_e}{2}}^{\frac{h_e}{2}} \frac{\nu E(z)}{1-\nu^2}\Big[\big(\frac{\partial u_0}{\partial r} + z\,\frac{\partial \theta_r}{\partial r} - \frac{4z^3}{3h^2}\big(\frac{\partial \theta_r}{\partial r} + \frac{\partial^2 w}{\partial r^2}\big)\big) \\
&\quad + \frac{E(z)}{1-\nu^2}\big(\frac{u_0}{r} + \frac{z\,\theta_r}{r} - \frac{4z^3}{3h^2 r}(\theta_r + \frac{\partial w}{\partial r})dz \;, \\
M_{\theta\theta}^{B} &= \int_{-\frac{h_e}{2}}^{\frac{h_e}{2}} \sigma_{\theta\theta}^{e} z\,dz = \int_{-\frac{h_e}{2}}^{\frac{h_e}{2}} \frac{z\,\nu E(z)}{1-\nu^2}\Big[\big(\frac{\partial u_0}{\partial r} + z\,\frac{\partial \theta_r}{\partial r} - \frac{4z^3}{3h^2}\big(\frac{\partial \theta_r}{\partial r} + \frac{\partial^2 w}{\partial r^2}\big)\big)dz \\
&\quad + \frac{zE(z)}{1-\nu^2}\big(\frac{u_0}{r} + \frac{z\,\theta_r}{r} - \frac{4z^3}{3h^2 r}(\theta_r + \frac{\partial w}{\partial r})dz \;, \\
P_{\theta\theta}^{B} &= \int_{-\frac{h_e}{2}}^{\frac{h_e}{2}} \sigma_{\theta\theta}^{e} z^3 dz = \int_{-\frac{h_e}{2}}^{\frac{h_e}{2}} \frac{z^3\nu E(z)}{1-\nu^2}\Big[\big(\frac{\partial u_0}{\partial r} + z\,\frac{\partial \theta_r}{\partial r} - \frac{4z^3}{3h^2}\big(\frac{\partial \theta_r}{\partial r} + \frac{\partial^2 w}{\partial r^2}\big)\big)dz \\
&\quad + \frac{z^3E(z)}{1-\nu^2}\big(\frac{u_0}{r} + \frac{z\,\theta_r}{r} - \frac{4z^3}{3h^2 r}(\theta_r + \frac{\partial w}{\partial r})dz \\
N_{rr}^{C} &= \int_{\frac{h_e}{2}}^{\frac{h_e}{2}+h_p} \sigma_{rr}^{p} dz = \int_{\frac{h_e}{2}}^{\frac{h_e}{2}+h_p} \Big[\bar{c}_{11}\big(\frac{\partial u_0}{\partial r} + z\,\frac{\partial \theta_r}{\partial r} - \frac{4z^3}{3h^2}\big(\frac{\partial \theta_r}{\partial r} + \frac{\partial^2 w}{\partial r^2}\big)\big) \\
&\quad + \bar{c}_{12}\big(\frac{u_0}{r} + \frac{z\,\theta_r}{r} - \frac{4z^3}{3h^2 r}(\theta_r + \frac{\partial w}{\partial r})\big) - \bar{e}_{31}E_z\Big]dz \;, \\
M_{rr}^{C} &= \int_{\frac{h_e}{2}}^{\frac{h_e}{2}+h_p} \sigma_{rr}^{p} z\,dz = \int_{\frac{h_e}{2}}^{\frac{h_e}{2}+h_p} \Big[\bar{c}_{11} z\,\big(\frac{\partial u_0}{\partial r} + z\,\frac{\partial \theta_r}{\partial r} - \frac{4z^3}{3h^2}\big(\frac{\partial \theta_r}{\partial r} + \frac{\partial^2 w}{\partial r^2}\big)\big) \\
&\quad + \bar{c}_{12} z\,\big(\frac{u_0}{r} + \frac{z\,\theta_r}{r} - \frac{4z^3}{3h^2 r}(\theta_r + \frac{\partial w}{\partial r})\big) - \bar{e}_{31} z E_z\Big]dz \;, \\
P_{rr}^{C} &= \int_{\frac{h_e}{2}}^{\frac{h_e}{2}++h_p} \sigma_{rr}^{p} z^3 dz = \int_{\frac{h_e}{2}}^{\frac{h_e}{2}+h_p} \Big[\bar{c}_{11} z^3\,\big(\frac{\partial u_0}{\partial r} + z\,\frac{\partial \theta_r}{\partial r} - \frac{4z^3}{3h^2}\big(\frac{\partial \theta_r}{\partial r} + \frac{\partial^2 w}{\partial r^2}\big)\big) \\
&\quad + \bar{c}_{12} z^3\big(\frac{u_0}{r} + \frac{z\,\theta_r}{r} - \frac{4z^3}{3h^2 r}(\theta_r + \frac{\partial w}{\partial r})\big) - \bar{e}_{31} z^3 E_z\Big]dz \\
N_{\theta\theta}^{C} &= \int_{\frac{h_e}{2}}^{\frac{h_e}{2}+h_p} \sigma_{\theta\theta}^{p} dz = \int_{\frac{h_e}{2}}^{\frac{h_e}{2}+h_p} \Big[\bar{c}_{21}\big(\frac{\partial u_0}{\partial r} + z\,\frac{\partial \theta_r}{\partial r} - \frac{4z^3}{3h^2}\big(\frac{\partial \theta_r}{\partial r} + \frac{\partial^2 w}{\partial r^2}\big)\big) \\
&\quad + \bar{c}_{22}\big(\frac{u_0}{r} + \frac{z\,\theta_r}{r} - \frac{4z^3}{3h^2 r}(\theta_r + \frac{\partial w}{\partial r})\big) - \bar{e}_{32}E_z\Big]dz \;, \\
M_{\theta\theta}^{C} &= \int_{\frac{h_e}{2}}^{\frac{h_e}{2}+h_p} \sigma_{\theta\theta}^{p} z\,dz = \int_{\frac{h_e}{2}}^{\frac{h_e}{2}+h_p} \Big[\bar{c}_{21} z\,\big(\frac{\partial u_0}{\partial r} + z\,\frac{\partial \theta_r}{\partial r} - \frac{4z^3}{3h^2}\big(\frac{\partial \theta_r}{\partial r} + \frac{\partial^2 w}{\partial r^2}\big)\big) \\
&\quad + \bar{c}_{22} z\,\big(\frac{u_0}{r} + \frac{z\,\theta_r}{r} - \frac{4z^3}{3h^2 r}(\theta_r + \frac{\partial w}{\partial r})\big) - \bar{e}_{32} z E_z\Big]dz \;, \\
P_{\theta\theta}^{C} &= \int_{\frac{h_e}{2}}^{\frac{h_e}{2}+h_p} \sigma_{rr}^{p} z^3 dz = \int_{\frac{h_e}{2}}^{\frac{h_e}{2}+h_p} \Big[\bar{c}_{21} z^3\,\big(\frac{\partial u_0}{\partial r} + z\,\frac{\partial \theta_r}{\partial r} - \frac{4z^3}{3h^2}\big(\frac{\partial \theta_r}{\partial r} + \frac{\partial^2 w}{\partial r^2}\big)\big) \\
&\quad + \bar{c}_{22} z^3\big(\frac{u_0}{r} + \frac{z\,\theta_r}{r} - \frac{4z^3}{3h^2 r}(\theta_r + \frac{\partial w}{\partial r})\big) - \bar{e}_{32} z^3 E_z\Big]dz \\
Q_{rz}^{C} &= \int_{\frac{h_e}{2}}^{\frac{h_e}{2}+h_p} \sigma_{rz}^{p} dz = \int_{\frac{h_e}{2}}^{\frac{h_e}{2}+h_p} \big(\bar{c}_{44}(1-\frac{4z}{h^2})(\theta_r + \frac{\partial w}{\partial r}) - \bar{e}_{15}E_r\big)dz \;, \\
R_{rz}^{C} &= \int_{\frac{h_e}{2}}^{\frac{h_e}{2}+h_p} \sigma_{rz}^{p} z^2 dz = \int_{\frac{h_e}{2}}^{\frac{h_e}{2}+h_p} \big(\bar{c}_{44} z^2(1-\frac{4z}{h^2})(\theta_r + \frac{\partial w}{\partial r}) - \bar{e}_{15} z^2 E_r\big)dz
\end{aligned}
\tag{A.6}
$$

On the other hand, the kinetic energy variation (Eq. (A.2)) can be rewritten as follows:

$$\delta T:\int_S \begin{bmatrix} I_0\left(\dot{u}_0\delta\dot{u}_0+\dot{w}\,\delta\dot{w}\right)+I_1\left(\dot{u}_0\delta\dot{\theta}_r+\dot{\theta}_r\delta\dot{u}_0\right)+I_2\dot{\theta}_r\delta\dot{\theta}_r- \\ I_3c_1\left(\dot{u}_0\delta\dot{\theta}_r+\dot{u}_0\partial\dfrac{\delta\dot{w}}{\partial r}+\dot{\theta}_r\delta\dot{u}_0+\delta\dot{u}_0\dfrac{\partial\dot{w}}{\partial r}\right) \\ -I_4c_1\left(2\dot{\theta}_r\delta\dot{\theta}_r+\dot{\theta}_r\partial\dfrac{\delta\dot{w}}{\partial r}+\delta\dot{\theta}_r\dfrac{\partial\dot{w}}{\partial r}\right)+I_6c_1^2\left(\dot{\theta}_r\delta\dot{\theta}_r+\dot{\theta}_r\partial\dfrac{\delta\dot{w}}{\partial r}+\delta\dot{\theta}_r\dfrac{\partial\dot{w}}{\partial r}+\dfrac{\partial\dot{w}}{\partial r}\delta\dfrac{\partial\dot{w}}{\partial r}\right)\end{bmatrix}dS \tag{A.7}$$

In which the terms $I_0, I_1, I_2$, $I_3$, $I_4$ and $I_6$ represent the inertia coefficients for FG piezoelectric sandwich annular plate, and are defined as:

$$\begin{aligned}
I_0 &= \int_{-\frac{h_e}{2}-h_p}^{-\frac{h_e}{2}} \rho^p dz + \int_{-\frac{h_e}{2}}^{\frac{h_e}{2}} \rho^e(z)dz + \int_{\frac{h_e}{2}}^{\frac{h_e}{2}+h_p} \rho^p dz\,,\\
I_1 &= \int_{-\frac{h_e}{2}-h_p}^{-\frac{h_e}{2}} \rho^p z dz + \int_{-\frac{h_e}{2}}^{\frac{h_e}{2}} \rho^e(z)z dz + \int_{\frac{h_e}{2}}^{\frac{h_e}{2}+h_p} \rho^p z dz\,,\\
I_2 &= \int_{-\frac{h_e}{2}-h_p}^{-\frac{h_e}{2}} \rho^p z^2 dz + \int_{-\frac{h_e}{2}}^{\frac{h_e}{2}} \rho^e(z)z^2 dz + \int_{\frac{h_e}{2}}^{\frac{h_e}{2}+h_p} \rho^p z^2 dz\,,\\
I_3 &= \int_{-\frac{h_e}{2}-h_p}^{-\frac{h_e}{2}} \rho^p z^3 dz + \int_{-\frac{h_e}{2}}^{\frac{h_e}{2}} \rho^e(z)z^3 dz + \int_{\frac{h_e}{2}}^{\frac{h_e}{2}+h_p} \rho^p z^3 dz\,,\\
I_4 &= \int_{-\frac{h_e}{2}-h_p}^{-\frac{h_e}{2}} \rho^p z^4 dz + \int_{-\frac{h_e}{2}}^{\frac{h_e}{2}} \rho^e(z)z^4 dz + \int_{\frac{h_e}{2}}^{\frac{h_e}{2}+h_p} \rho^p z^4 dz\,,\\
I_6 &= \int_{-\frac{h_e}{2}-h_p}^{-\frac{h_e}{2}} \rho^p z^6 dz + \int_{-\frac{h_e}{2}}^{\frac{h_e}{2}} \rho^e(z)z^6 dz + \int_{\frac{h_e}{2}}^{\frac{h_e}{2}+h_p} \rho^p z^6 dz
\end{aligned} \tag{A.8}$$

## APPENDIX B

$$\{A_{11},A_{12},A_{44}\} = \int_{-\frac{h_e}{2}-h_p}^{-\frac{h_e}{2}} \{\bar{c}_{11},\bar{c}_{12},\bar{c}_{44}\}dz + \int_{-\frac{h_e}{2}}^{\frac{h_e}{2}} \frac{E(z)}{1-\nu^2}\left\{1,\nu,\frac{1-\nu}{2}\right\}dz + \int_{\frac{h_e}{2}}^{\frac{h_e}{2}+h_p} \{\bar{c}_{11},\bar{c}_{12},\bar{c}_{44}\}dz\,,$$

$$\{B_{11},B_{12},B_{44}\} = \int_{-\frac{h_e}{2}-h_p}^{-\frac{h_e}{2}} \{\bar{c}_{11},\bar{c}_{12},\bar{c}_{44}\}zdz + \int_{-\frac{h_e}{2}}^{\frac{h_e}{2}} \frac{E(z)}{1-\nu^2}z\left\{1,\nu,\frac{1-\nu}{2}\right\}dz + \int_{\frac{h_e}{2}}^{\frac{h_e}{2}+h_p} \{\bar{c}_{11},\bar{c}_{12},\bar{c}_{44}\}zdz\,,$$

$$\{E_{11},E_{12},E_{44}\} = \int_{-\frac{h_e}{2}-h_p}^{-\frac{h_e}{2}} \{\bar{c}_{11},\bar{c}_{12},\bar{c}_{44}\}z^2dz + \int_{-\frac{h_e}{2}}^{\frac{h_e}{2}} \frac{E(z)}{1-\nu^2}z^2\left\{1,\nu,\frac{1-\nu}{2}\right\}dz + \int_{\frac{h_e}{2}}^{\frac{h_e}{2}+h_p} \{\bar{c}_{11},\bar{c}_{12},\bar{c}_{44}\}z^2dz\,,$$

$$\{D_{11},D_{12},D_{44}\} = \int_{-\frac{h_e}{2}-h_p}^{-\frac{h_e}{2}} \{\bar{c}_{11},\bar{c}_{12},\bar{c}_{44}\}z^3dz + \int_{-\frac{h_e}{2}}^{\frac{h_e}{2}} \frac{E(z)}{1-\nu^2}z^3\left\{1,\nu,\frac{1-\nu}{2}\right\}dz + \int_{\frac{h_e}{2}}^{\frac{h_e}{2}+h_p} \{\bar{c}_{11},\bar{c}_{12},\bar{c}_{44}\}z^3dz\,,$$

## REFERENCES


[1] Liu X., Wang Q., Quek S.T., 2002, Analytical solution for free vibration of piezoelectric coupled moderately thick circular plates, *International Journal of Solids and Structures* **39**: 2129-2151.

[2] Dash P., Singh B.N., 2009, Nonlinear free vibration of piezoelectric laminated composite plate, *Finite Elements in Analysis and Design* **45**: 686-694.

[3] Phung-Van P., De Lorenzis L., Thai C.H., 2015, Analysis of laminated composite plates integrated with piezoelectric sensors and actuators using higher-order shear deformation theory and isogeometric finite elements, *Computational Materials Science* **96**: 495-505.

[4] Kuang J-H., Hsu C-M., Lin A-D., 2016, Determination of piezoelectric parameters from the measured natural frequencies of a piezoelectric circular plate, *Integrated Ferroelectrics* **168**: 36-52.

[5] Shu H., Liu W., Li S., 2016, Research on flexural wave band gap of a thin circular plate of piezoelectric radial phononic crystals, *Journal of Vibration and Control* **22**: 1777-1789.

[6] Khorshidvand A.R., Joubaneh E.F., Jabbari M., 2014, Buckling analysis of a porous circular plate with piezoelectric sensor–actuator layers under uniform radial compression, *Acta Mechanica* **225**: 179-193.

[7] Farzaneh Joubaneh E., Mojahedin A., Khorshidvand A., 2015, Thermal buckling analysis of porous circular plate with piezoelectric sensor-actuator layers under uniform thermal load, *Journal of Sandwich Structures and Materials* **17**: 3-25.

[8] Duc N.D., Cong P.H., Quang V.D., 2016, Nonlinear dynamic and vibration analysis of piezoelectric eccentrically stiffened FGM plates in thermal environment, *International Journal of Mechanical Sciences* **115-116**: 711-722.

[9] Hayashi M., Koyama D., Matsukawa M., 2016, Piezoelectric particle counter using the resonance vibration modes of a circular plate, *Journal of the Acoustical Society of America* **140**: 3035-3035.

[10] Arefi M., 2015, Nonlinear electromechanical stability of a functionally graded circular plate integrated with functionally graded piezoelectric layers, *Latin American Journal of Solids and Structures* **12**: 1653-1665.

[11] Fesharaki J.J., Madani S.G., Golabi S., 2017, Investigating the effect of stiffness/thickness ratio on the optimal location of piezoelectric actuators through PSO algorithm, *Journal of Solid Mechanics* **9**: 832-848.

[12] Karami Khorramabadi M., 2009, Free vibration of functionally graded beams with piezoelectric layers subjected to axial load, *Journal of Solid Mechanics* **1**: 22-28.

[13] Mohammadimehr M., Mohandes M., 2015, The effect of modified couple stress theory on buckling and vibration analysis of functionally graded double-layer boron nitride piezoelectric plate based on CPT, *Journal of Solid Mechanics* **7**: 281-298.

[14] Hosseini M., Bahreman M., Jamalpoor A., 2017, Thermomechanical vibration analysis of FGM viscoelastic multi-nanoplate system incorporating the surface effects via nonlocal elasticity theory, *Microsystem Technologies* **23**: 3041-3058.

[15] Bhangale R.K., Ganesan N., 2005, Free vibration studies of simply supported non-homogeneous functionally graded magneto-electro-elastic finite cylindrical shells, *Journal of Sound and Vibration* **288**: 412-422.

[16] Yang T., Zheng W., Huang Q., 2016, Sound radiation of functionally graded materials plates in thermal environment, *Composite Structures* **144**: 165-176.

[17] Su Z., Jin G., Ye T., 2018, Electro-mechanical vibration characteristics of functionally graded piezoelectric plates with general boundary conditions, *International Journal of Mechanical Sciences* **138-139**: 42-53.

[18] Kiani Y., 2016, Free vibration of functionally graded carbon nanotube reinforced composite plates integrated with piezoelectric layers, *Computers & Mathematics with Applications* **72**: 2433-2449.

[19] Barati M.R., Zenkour A.M., 2018, Electro-thermoelastic vibration of plates made of porous functionally graded piezoelectric materials under various boundary conditions, *Journal of Vibration and Control* **24**: 1910-1926.

[20] Seibert H.F., 2006, Applications for PMI foams in aerospace sandwich structures, *Reinforced Plastics* **50**: 44-48.

[21] Natarajan S., Haboussi M., Manickam G., 2014, Application of higher-order structural theory to bending and free vibration analysis of sandwich plates with CNT reinforced composite facesheets, *Composite Structures* **113**: 197-207.

[22] Santos Silva J., Dias Rodrigues J., Moreira R.A.S., 2010, Application of cork compounds in sandwich structures for vibration damping, *Journal of Sandwich Structures and Materials* **12**: 495-515.

[23] Vinson J.R., 2001, Sandwich structures, *Applied Mechanics Reviews* **54**: 201.

[24] El Meiche N., Tounsi A., Ziane N., 2011, A new hyperbolic shear deformation theory for buckling and vibration of functionally graded sandwich plate, *International Journal of Mechanical Sciences* **53**: 237-247.

[25] Hadji L., Atmane H.A., Tounsi A., 2011, Free vibration of functionally graded sandwich plates using four-variable refined plate theory, *Applied Mathematics and Mechanics* **32**: 925-942.

[26] Dinh Duc N., Hong Cong P., 2018, Nonlinear thermo-mechanical dynamic analysis and vibration of higher order shear deformable piezoelectric functionally graded material sandwich plates resting on elastic foundations,*Journal of Sandwich Structures and Materials* **20**: 191-218.

[27] Alibeigloo A., 2017, Three dimensional coupled thermoelasticity solution of sandwich plate with FGM core under thermal shock, *Composite Structures* **177**: 96-103.

[28] Fatahi-Vajari A., Imam A., 2016, Lateral vibrations of single-layered graphene sheets using doublet mechanics, *Journal of Solid Mechanics* **8**: 875-894.

[29] Fazzolari F.A., 2016, Stability analysis of FGM sandwich plates by using variable-kinematics Ritz models, *Mechanics of Advanced Materials and Structures* **23**: 1104-1113.

[30] Arefi M., Mohammad-Rezaei Bidgoli E., Zenkour A.M., 2018, Free vibration analysis of a sandwich nano-plate including FG core and piezoelectric face-sheets by considering neutral surface, *Mechanics of Advanced Materials and Structures* **2018**: 1-12.

[31] Hosseini M., Jamalpoor A., 2015, Analytical solution for thermomechanical vibration of double-viscoelastic nanoplate-systems made of functionally graded materials, *Journal of Thermal Stresses* **38**: 1428-1456.

[32] Sahmani S., Bahrami M., Ansari R., 2014, Surface effects on the free vibration behavior of postbuckled circular higher-order shear deformable nanoplates including geometrical nonlinearity, *Acta Astronautica* **105**: 417-427.

[33] Ansari R., Torabi J., Hasrati E., 2018, Axisymmetric nonlinear vibration analysis of sandwich annular plates with FG-CNTRC face sheets based on the higher-order shear deformation plate theory, *Aerospace Science and Technology* **77**: 306-319.

[34] Ashoori A.R., Vanini S.A.S., Salari E., 2017, Size-dependent axisymmetric vibration of functionally graded circular plates in bifurcation/limit point instability, *Applied Physics A* **123**: 226.

[35] Arefi M., Zamani M., Kiani M., 2018, Size-dependent free vibration analysis of three-layered exponentially graded nanoplate with piezomagnetic face-sheets resting on Pasternak's foundation, *Journal of Intelligent Materials Systems and Structures* **29**: 774-786.

[36] Mohammadimehr M., Emdadi M., Afshari H., 2017, Bending, buckling and vibration analyses of MSGT microcomposite circular-annular sandwich plate under hydro-thermo-magneto-mechanical loadings using DQM, *International Journal of Smart and Nano Materials* **2017**: 1-28.

[37] Eshraghi I., Dag S., Soltani N.,2015, Consideration of spatial variation of the length scale parameter in static and dynamic analyses of functionally graded annular and circular micro-plates, *Composites Part B: Engineering* **78**: 338-348.

[38] Liew K.M., Xiang Y., Kitipornchai S., 2018, *Vibration of Mindlin Plates : Programming the P-Version Ritz Method*, Elsevier.

[39] Ebrahimi F., Rastgoo A., 2008, Free vibration analysis of smart annular FGM plates integrated with piezoelectric layers, *Smart Materials and Structures* **17**: 015044.